PROFESSOR ZHENJIE FENG (Orcid ID : 0000-0001-5870-5159)

Article type : Article

Selenium-doping induced two antiferromagnetic transitions in thiospinel compounds $CuCo_2S_{4-x}Se_x$ ($0 \le x \le 0.8$)

Zhenjie Feng[1, 2, 3*], Qiang Hou[1], Tao Li[1], Ke Wang[1], Hao Wu[1], Jingying Si[1], Wenlai Lv, Jun-Yi Ge[1], Shixun Cao[1,2], Jincang Zhang[1], Nai-Chang Yeh[4*]

[1]*Materials Genome Institute, Department of Physics, Shanghai University, Shanghai, 200444, China*

[2]*Shanghai Key Laboratory of High Temperature Superconductors, Shanghai 200444, China*

[3]*Shanghai Laue Sci & Tech Center, Shanghai, 200444, China*

[4]*Department of Physics, California Institute of Technology, Pasadena, CA 91125, USA*

Abstract: A series of copper thiospinels compounds, $CuCo_2S_{4-x}Se_x$ (x = 0, 0.2, 0.4, 0.6, 0.8), have been successfully synthesized by solid state reaction and their structure and magnetic properties have been studied. The Rietveld refinements of X-Ray diffractions indicate that both the lattice constants and the nearest neighbor Cu-Cu distances increase with increasing selenium doping. A weakly antiferromagnetic transition occurring at about 4 K is observed in $CuCo_2S_4$. Two antiferromagnetic transitions at about 3.5 K and 6 K are observed in selenium-doped samples, which suggest that the exchange couplings associated with Cu-S(Se)-Cu and Cu-Se(S)-Cu, respectively, are responsible for the two antiferromagnetic transitions. Detailed analysis of the experimental results further indicate that the nearest-neighbor molecular field coefficient is comparable to the next-neighbor molecular field coefficient. We propose a reasonable model to explain this phenomenon.

Corresponding Author: fengzhenjie@shu.edu.cn, ncyeh@caltech.edu

This article has been accepted for publication and undergone full peer review but has not been through the copyediting, typesetting, pagination and proofreading process, which may lead to differences between this version and the Version of Record. Please cite this article as doi: 10.1111/JACE.17607

KEYWORDS : $CuCo_2S_4$, thiospinels, crystal structure, antiferromagnetism

1. INTRODUCTION

Copper thiospinels, CuM_2S_4 (M = Co, Rh, Ir, Cr, *etc.*), have attracted considerable attention due to their rich physical and chemical properties, such as superconductivity, magnetic order, metal-insulator transition, thermoelectric and catalytic effects. The crystalline structure of the copper thiospinels is consistent with the structure of spinels with a general formula of AB_2X_4 and the space group is $Fd\bar{3}m$. Among the copper thiospinels, $CuRh_2S_4$ is the first superconductor found in thiospinels, and its critical temperature is 4.7 K.[1] A metal-insulator transition at 230 K[2] as well as charge ordering and atomic dimerization[3] have been observed in $CuIr_2S_4$. Colossal magnetoresistance (CMR) and a relatively high Curie temperature at 380 K has been found in $CuCr_2S_4$.[4] Nanoparticles of $CuCo_2S_4$ are active electro-catalytic materials with excellent electrochemical performance, which are promising for use as electrode materials in supercapacitors.[5, 6] Additionally, the photo stability and high photo-thermal performance of $CuCo_2S_4$ may play a role in photothermal treatment of cancer.[7] Recently, $CuCo_2S_4$ has also been shown to be a promising eco-friendly thermoelectric material.[8]

The $CuCo_2S_4$ compound belongs to a spinel structure with the tetrahedral A-site occupied by Cu^{2+} and the octahedral B-site occupied by Co^{3+}, as shown in Figure 1(a). It is known to exhibit weak antiferromagnetism at low temperature from nuclear magnetic resonance (NMR) studies.[9–11] The Co^{3+} ($3d^6$) ion is in a nonmagnetic low spin state so that the magnetism in $CuCo_2S_4$, especially its antiferromagnetism, originates from the Cu^{2+} ($3d^9$).[10] When excess copper substitutes for the cobalt site, superconductivity with a transition temperature (T_c) ranging from 2 K to 4 K appears in $Cu_{1+x}Co_{2-x}S_4$ ($0 \leq x \leq 0.5$), and the T_c value increases with increasing copper content.[12] Interestingly, both superconductivity and antiferromagnetism have been found in $Cu_{1+x}Co_{2-x}S_4$ ($0 < x \leq 0.5$), where the excess Cu^{2+} ions enter the octahedral B-site. On the other hand, no antiferromagnetism is found in $Cu_{1.3}K_{0.2}Co_{1.5}S_4$,[13] suggesting that antiferromagnetism disappears when K^+ ions replace some of the Cu^{2+} in the B-site. In others words, the antiferromagnetic interaction of Cu-S-Cu is destroyed by the interaction of Cu-S-K. Although these element substitutions at the B-site cause lattice distortion, the low spin state of Co^{3+} ($3d^6$) is not affected by the substitutions. Considering the origin of antiferromagnetism, it will be interesting to investigate the effect of Se substitution for S, which will lead to perturbations to the vertex sites of the octahedral (see Figure 1(a)), thereby modifying the superconductivity and magnetism in this spinel system.

In this work, we report our successful synthesis of $CuCo_2S_{4-x}Se_x$ (x = 0, 0.2, 0.4, 0.6, 0.8), in which S is substituted by Se with different contents. We find that both the lattice constants of $CuCo_2S_{4-x}Se_x$ and the atom distances of Cu-S(Se) become larger with increasing doping level x according to calculations of Rietveld refinement. Two antiferromagnetic transitions are observed in selenium-doped samples, which may be attributed to two different antiferromagnetic interactions associated with Cu-S(Se)-Cu and Cu-Se(S)-Cu while the low spin state of Co^{3+} ($3d^6$) remains unaffected by the Se substitution. Here the expression Cu-S(Se)-Cu refers to a local region where the amount of Sulphur atoms is more than that of selenium atoms, and vice versa for the expression Cu-Se(S)-Cu.

2. EXPERIMENTAL PROCEDURE

Solid solution of $CuCo_2S_{4-x}Se_x$ was prepared by traditional solid state reaction with the following starting materials: CuS (> 99 %), Co (99.5 %), S (99.999 %) and Se (99.99 %). Raw materials with stoichiometric proportions were first mixed together and grinded evenly. The mixture was pressed into a pellet and then sealed in a vacuum quartz tube. Next, the quartz tube was heated to 300 °C at 2 °C/min, and then kept at 300 °C for 4 hours in order to prevent Se and S from volatilizing at higher temperature that could lead to the appearance of impurities and even explosion of the quartz tube. Subsequently, the quartz tube was further heated to 750 °C at 2 °C/min and kept at 750 °C for two days. Finally, the furnace was turned off to allow cooling of the sample back to room temperature.

The powder diffraction data were obtained by using the x-ray diffractometer (D2 PHASER, BRUKER) with a wavelength λ = 1.54 Å of the Cu-Kα radiation and an energy dispersive LYNXEYE XE-T linear detector at the continuous scanning mode. The Rietveld refinement is carried out by the GSASII software.[14] The morphology of samples was characterized by the Scanning Electron Microscope (SEM,SU5000, Hitachi). The magnetic properties were measured by the Physical Property Measurement System (PPMS DynaCool, Quantum Design) and the Magnetic Property Measurement System (MPMS 3, Quantum Design).

3. RESULTS AND DISCUSSION

3.1 The crystal structure analysis

Figure 2 (a) shows the X-ray diffraction (XRD) patterns of all $CuCo_2S_{4-x}Se_x$ samples with different selenium

doping levels (x = 0, 0.2, 0.4, 0.6, 0.8) at room temperature in air. The Rietveld refinements of X-Ray diffractions indicate that all compounds are spinel-type single phases with the space group $Fd\bar{3}m$. The corresponding factors of all the Rietveld refinements are listed in the table 1, where R_{wp} represents the overall weighted profile R factor; GOF represents the goodness-of-fit, aka square root of the reduced χ^2 (in this paper,); R_F means the final refinement R_F on 28 or 29 reflections. All the R_{wp} are good enough for the acceptance. The value of R_{wp} slightly gradually increases with doping level x increases, which may indicate very small impurity is slightly growing, although no impurity peaks are observed in the powder diffraction patterns. When x is more than 1, then the impurity peaks can be observed obviously. One of the final Rietveld refinements result for x = 0.2 is shown in Figure 2 (b). Additionally, both the nearest neighbor Cu-Cu distances and the lattice constants are found to increase linearly with the selenium doping, as shown in Figure 2 (c) and (d), respectively. These findings are reasonable because of the bigger radius of the Se dopant. We further note that the lattice parameter of $CuCo_2S_4$ as determined from this work is consistent with the values of a = 9.4504 Å[12] and a = 9.4640 Å[15] reported previously.

For $CuCo_2S_{4-x}Se_x$ samples with higher Se content (x > 0.8), however, we found that a second phase appeared. Specifically, a set of impurity peaks may be associated with copper-sulfur or cobalt-sulfur binary compounds. The other set of peaks were consistent with the diffraction peaks of the standard spinel $CuCo_2S_4$, with offsets of the main diffraction peaks indicative of the presence of the Se element in the lattice. It is worth mentioning that the conditions for synthesizing $CuCo_2S_{4-x}Se_x$ are very strict, and samples with higher Se content, especially $CuCo_2Se_4$, cannot be obtained by our current method. Therefore, in this work we limit our investigation of $CuCo_2S_{4-x}Se_x$ to pure samples with x < 1.

3.2 **Morphology analysis**

Figure 3 (a) and (b) show the SEM images of $CuCo_2S_4$ with different magnification of × 1.00 k and × 10.00 k. The morphology is mostly consistent with the SEM images given in Reference [8] except for the grain sizes, which were ~ 200 nm in Reference "8" and ~ 1 μm in this work (Figure 3 (b)). The smaller grain size reported previously may be the result of additional sample processing by ball-milling and spark plasma sintering (SPS) after solid-state reaction "8", whereas our sample processing only involved solid-state reaction.

Figure 3 (c-f) shows the SEM images of the $CuCo_2S_{4-x}Se_x$ compounds with different selenium doping

levels. Obviously, there is not much difference between doping samples (x = 0.2, 0.4, 0.6, 0.8) and parent phase $CuCo_2S_4$. However, the conductivity of selenium-doped compounds appeared to have decreased relative to the parent compound, because the SEM images of the selenium-doped compounds could not be imaged with as high magnification as those of $CuCo_2S_4$.

3.3 Magnetic properties

Figure 4 (a) shows the magnetic susceptibility (χ) *vs.* temperature (from 2 to 60 K) data of $CuCo_2S_{4-x}Se_x$ (x = 0, 0.2, 0.4, 0.6, 0.8) samples in ZFC (Zero Field Cooled) and FC (Field Cooled) modes under an external-field H = 200 Oe, and the inset shows the ZFC curves for temperatures from 2 to 10 K. In Figure 4 (b) the ZFC data of $1/\chi$ are shown as a function of temperature from 2 to 60 K, and the fitting curves using the Curie-Weiss law are indicated by the white solid lines. Both the Néel temperature and the magnetic susceptibility are found to vary with Se doping: A very weakly antiferromagnetic transition (T_{N1}) of the parent phase $CuCo_2S_4$ is observed at 3.86 K. The Néel temperature T_{N1} reaches a maximum value of 6.39 K when x = 0.4, and then decreases with Se doping when x > 0.4. Additionally, a new antiferromagnetic transition (T_{N2}) appears at 2.67 K when x = 0.4, and T_{N2} continues to increase with x and finally reaches 3.5 K for x = 0.8. The results in Figure 4 (a) - (b) are obtained from the PPMS instrument. If the applied external magnetic field is relatively small for these compounds, the measurement signals are very close to the measurement limit of PPMS, which will result in severe data jitter. In order to eliminate the jitter, a relatively large external magnetic field, H = 200 Oe is used to obtained these data on the PPMS instrument. In order to observe the antiferromagnetic transition clearly, we took the measurements of the temperature-dependent DC susceptibility (χ) for x = 0.4 and x = 0.6 samples on MPMS with external field H = 20, and added the results in Figure 4 (c). The two antiferromagnetic transitions could be observed clearly in Figure 4 (c). Both features around 3.5 K and 6 K are more prominent in ZFC mode at lower magnetic field and show peaks at particular temperatures for each compound. This indicates that the both peaks correspond to antiferromagnetic transition as the peaks are getting reduced at higher field such as 200 Oe (in the inset of Figure 4 (a)). In order to further clarify if the two transition points should be attributed to antiferromagnetic characters, we carried out the isothermal magnetic hysteresis loop measurements for two samples, x= 0.4 and 0.6, at 2 K, 4 K, 6 K and 10k, respectively, as shown in Figure 4 (d) and 4 (e). These raw hysteresis loops overlap seriously. In order to show these loops clearly, we increase the M values of the curves

of 4K, 6K and 10K by 0.1, 0.2 and 0.3, respectively. The antiferromagnetic curves demonstrated at 2 and 4 K indicate the pure antiferromagnetic region below 6 K. The character of the antiferromagnetic hysteresis loop becomes weaker with temperature increase. The plot at 6 K also shows the antiferromagnetic curve but with less prominent character as the random spins in paramagnetic region cannot be arranged immediately in the antiferromagnetic ordering just below the Néel temperature. Finally, the plots at 10 K (above Néel temperature) exhibit the paramagnetic ordering. Hence both the transition temperatures from magnetic susceptibility curve can be attributed to the antiferromagnetic ordering. However, the bifurcation between ZFC and FC curves around the Néel temperature may suggest the spin glass nature which must be verified before reaching any conclusion.

In order to exclude the possibility of the spin glass transition. We measured Alternating current (AC) susceptibility (χ_{ac}) response in 6 Oe AC field for various values of frequency in the magnetically ordered state and plotted the temperature dependence of the real part (χ_{ac}') in the absence of dc magnetic field for x = 0.4 and 0.6 in the Figure 5 (a) and (b). There are two features observed similar like DC susceptibility plots around the two antiferromagnetic transition temperatures for both compositions. However, they do not show any noticeable frequency-dependence shift of the observed features which clearly ruled out the possibility of spin glass freezing at these temperatures. It can be therefore concluded that the evolution of the antiferromagnetic ordering is solely responsible for these transitions.

The relationship between the Néel temperatures and the selenium doping level is summarized in Figure 6 (a). It is obvious that the Néel temperature T_{N1} is the highest at x = 0.4, where the second antiferromagnetic transition T_{N2} emerges. To better understand the effect of Se doping on the magnetic properties of $CuCo_2S_{4-x}Se_x$, we examine the magnetic susceptibility of samples by fitting the high-temperature data to the Curie-Weiss law:

$$\chi = {}^{C}/_{(T - T_P)}, \qquad (1)$$

where C represents the Curie constant and T_P denotes the asymptotic (or paramagnetic) Curie temperature. The fitting results of C and T_p for different Se-doping levels are shown in Figure 6 (b). The effective Bohr magneton μ_{eff} derived from the Curie-Weiss fitting is shown in Table 2. Low spin state of $Co^{3+}(3d^6)$ has been proved by nuclear magnetic resonance experiments[10, 11]. The low spin state of Co^{3+} has a very strong correlation with the high symmetry octahedral in $CuCo_2S_4$ spinel structure. The radius difference of doped Se to S position will result in the distortion of the octahedral. It is reasonable to conclude that big enough distortion will change a low

spin state to a middle or a high spin state. The effective Bohr magneton is the total magnetic moment of each formula. As shown in table 2, the calculated effective Bohr magnetons μ_{eff} for $x \geq 0.2$ samples are a little bigger than that for x = 0 sample, which may indicate that some low spin states change to middle or high spin state in some uneven doping areas. However, the effective Bohr magnetons does not increase greatly and still remains around 1, which indicates that most of the $Co^{3+}(3d^6)$ ions keep their low spin state with Se doping increase. Therefore, the effective Bohr magneton is from the Cu^{2+} ions in these compounds. We also note that the effective moment is consistent with the Cu^{2+} ions, which increases upon Se doping. For x = 0.4, both the Curie constant C and the paramagnetic Curie temperature T_P are the largest. Inasmuch as T_P is proportional to the molecular field coefficient, it means that the molecular field reaches a maximum value when x = 0.4. The obvious change in the orbital magnetic moment is due to different degrees of overlap of the electron cloud between Cu and Se, which are determined by the Cu-S/Se distance and the Se content. The higher Se content and the smaller the Cu-S/Se distance, the greater overlap of the electron cloud between Cu and Se, hence the larger value of μ_{eff}. Thus, the effective magnetic moment is the largest when x = 0.4. In Table 3 we summarize the data of lattice parameters, paramagnetic Curie temperatures and Néel temperatures.

There are five kinds of super-exchange interactions in the thiospinel structure: AB(NN), BB(NN), AB(NNN), BB(NNN) and AA(NN), (NN: nearest-neighbor, and NNN: next-nearest-neighbor), as shown in Figure 1 (b). In the case of $CuCo_2S_4$, Co^{3+} ($3d^6$) is in the nonmagnetic low spin state so that magnetism in the sample originates from Cu^{2+} ($3d^9$).[9] Therefore, the antiferromagnetic super-exchange interaction can only be mediated by Cu-S(Se)-Cu interaction, namely AA(NN) super-exchange interaction in Figure 1 (b), and the molecular field reaches the maximum at x = 0.4 due to the strongest super-exchange interactions between Cu-S(Se)-Cu. Empirically, the AA(NN) super-exchange interaction increases with x when $x < 0.4$, reaches the maximum value at x = 0.4, then decreases when $x > 0.4$. Meanwhile, the second antiferromagnetic interaction emerges when $x \geq 0.4$. A feasible scenario for the observed phenomena is as follows: (1) When $x < 0.4$, the doping of larger Se atoms provides more overlaps in the electronic clouds, which strengthens the super-exchange interaction in Cu-S(Se)-Cu while the Cu-Cu distance does not exhibit significant increase. Therefore, the super-exchange interaction becomes stronger, which is reflected on the increase of both the Curie constant (C) and the paramagnetic Curie temperature (T_p) with Se doping. (2) When $x > 0.4$, the increase in the Cu-Cu distance dominates over the benefits of larger Se atoms. Therefore, both the C and T_p decrease with Se doping.

(3) When $x \geq 0.4$, interactions associated with Cu-Se(S)-Cu begin to emerge, giving rise to a new antiferromagnetic transition at T_{N2} . Furthermore, the trend of T_{N1} and T_{N2} should merge at some doping level if samples with purely Cu-S(Se)-Cu and Cu-Se(S)-Cu interactions could be obtained. Of course, there is only Cu-S-Cu super-exchange in the parent compound $CuCo_2S_4$.

The main super-exchange interaction results from Cu-S(Se)-Cu. According to molecular field theory,[16, 17] there are two localized molecular fields in antiferromagnetic materials, which can be manifested by the following formulas:

$$T_P = \frac{1+\alpha}{1-\alpha} T_N, \ (\alpha = \frac{\lambda_{ii}}{\lambda_{AB}}). \quad (2)$$

Here λ_{AB} denotes the nearest-neighbor (NN) molecular field constant and λ_{ii} is the next-nearest-neighbor (NNN) molecular field constant. For every sample, we calculate the coefficient α by using Eq. (2) with the fitted T_p value derived from EQ. (1) and the experimental T_N value identified from the χ-*vs.*-T curve. The doping dependent coefficient α thus obtained is summarized in Table 4. Interestingly, we found that all coefficients α are very close to 1.0, which means that the nearest-neighbor molecular field constant, λ_{AB}, is essentially equal to the next-neighbor molecular field constant, λ_{ii}. From the crystal structure, the nearest-neighbor (NN) copper-copper distance is about 4.10 Å and the next-nearest-neighbor (NNN) copper-copper distance is about 7.86 Å. Therefore, it is unlikely for the NNN copper-copper interaction to be equal to the NN copper-copper interaction.

An alternative and feasible interpretation for the finding of $\alpha \approx 1$ is that there are two types of NN copper-copper interactions in the $CuCo_2S_{4-x}Se_x$ compounds. One is associated with the Cu-S(Se)-Cu interaction, and the other is associated with the Cu-Se(S)-Cu interaction. Under this scenario, it becomes reasonable for $\alpha \approx 1$ and $\lambda_{AB} \approx \lambda_{ii}$. We have further calculated the angles of Cu-S(Se)-Cu for all doping levels by Rietveld refinement, which are summarized in Table 4 together with the corresponding coefficients α. We find that the angles of Cu-S(Se)-Cu in all samples are all about 77.7°, and the change rate of the angle is about 0.3%, which exceeds the resolution from Rietveld refinement. Additionally, we have calculated the Cu-S(Se) distance by Rietveld refinement, as shown in Figure 6 (c). We find that the Cu-S(Se)-Cu distance generally increases with Se doping except at x = 0.4 where the Cu-S(Se)-Cu distance exhibits a decrease. Comparing the NN Cu-S(Se)-Cu distance and the Cu-S(Se)-Cu angle, we find that the Cu-S(Se)-Cu distance has more influence on the magnetic properties so that the magnitude of the distance as a function of Se-doping correlates well with the

values of the Curie constant C and the paramagnetic Curie temperature T_p, with an extreme found at $x = 0.4$. Additionally, the scenario of two types of NN copper-copper interactions in the $CuCo_2S_{4-x}Se_x$ compounds is consistent with our finding of two antiferromagnetic transitions: The first transition is due to the super-exchange interaction of Cu-S(Se)-Cu, whereas the second transition when $x \geq 0.4$ is due to the effect of Cu-Se(S)-Cu interaction.

4. CONCLUSIONS Conclusion

We have successfully prepared a series of copper thiospinels compounds, $CuCo_2S_{4-x}Se_x$ (x = 0, 0.2, 0.4, 0.6, 0.8), and found that the antiferromagnetic interaction is enhanced with Se doping. The Co^{3+} ($3d^6$) ion is in a nonmagnetic low spin state in this system so that antiferromagnetism in the parent compound $CuCo_2S_4$ mainly results from Cu^{2+} ($3d^9$). With increasing Se doping, an additional antiferromagnetic transition emerges for $x \geq 0.4$, which may be attributed to two types of nearest-neighbor Cu-Cu interactions due to varying Cu-S(Se)-Cu and Cu-Se(S)-Cu distances with Se doping according to the Rietveld refinements of x-ray diffraction data. It is concluded that the addition of Se results in a new antiferromagnetic coupling of Cu^{2+} ($3d^9$) in $CuCo_2S_{4-x}Se_x$ and the Néel temperatures are sensitive to the contents of sulfur or selenium.

ACKNOWLEDGMENTS

This work at the Shanghai University (SHU) is jointly supported by the Ministry of Science and Technology of the People's Republic of China 2016YFB0700201, National Natural Science Foundation of China (11774217, 10904088), Shanghai Pujiang Program (13PJD015), and Science and Technology commission of Shanghai Municipality (13ZR1415200). N.-C. Yeh acknowledges the research support from the National Science Foundation (Award #1733907) and the Army Research Office (Award #W911NF-16-1-0472) in United States, and the hospitality and sponsorship of her visit to the SHU under the Overseas Expert Recruitment Program at SHU.

REFERENCES

1. Robbins M, Willens RH, Miller RC. Superconductivity in the spinels $CuRh_2S_4$ and $CuRh_2Se_2$. *Solid State*

Commun. 1967;5(12):933–934.

2. Nagata S, Hagino T, Seki Y, Bitoh T. Metal-insulator transition in thiospinel $CuIr_2S_4$. *Physica B*. 1994;194–196:1077–1078.
3. Radaelli PG, Horibe Y, Gutmann MJ, *et al.* Formation of isomorphic Ir^{3+} and Ir^{4+} octamers and spin dimerization in the spinel $CuIr_2S_4$. *Nature*. 2002;416(6877):155–158.
4. Lotgering FK. Ferromagnetism in spinels: $CuCr_2S_4$ and $CuCr_2Se_4$. *Solid State Commun*. 1964;2(2):55–56.
5. Wiltrout AM, Read CG, Spencer EM, Schaak RE. Solution Synthesis of Thiospinel $CuCo_2S_4$ Nanoparticles. *Inorg Chem*. 2016;55(1):221–226.
6. Cheng S, Shi T, Chen C, *et al.* Construction of porous $CuCo_2S_4$ nanorod arrays via anion exchange for high-performance asymmetric supercapacitor. *Scientific Reports*. 2017;7(1):6681.
7. Li B, Yuan F, He G, *et al.* Ultrasmall $CuCo_2S_4$ Nanocrystals: All-in-One Theragnosis Nanoplatform with Magnetic Resonance/Near-Infrared Imaging for Efficiently Photothermal Therapy of Tumors. *Adv Funct Mater*. 2017;27(10):1606218.
8. Lang Y, Pan L, Chen C, Wang Y. Thermoelectric Properties of Thiospinel-Type $CuCo_2S_4$. *J Electron Mater*. 2019;48(7):4179–4187.
9. Furukawa Y, Wada S, Miyatani K, Tanaka T, Fukugauchi M, Ishikawa M. Nuclear spin-lattice relaxation and antiferromagnetic spin correlations in superconducting thiospinel $Cu_{1.5}Co_{1.5}S_4$. *Phys Rev B*. 1995;51(9):6159–6162.
10. Wada S, Sugita H, Miyatani K, Tanaka T, Nishikawa T. Weak antiferromagnetism and superconductivity in pseudo-binary spinel compounds $(Cu,Co)Co_2S_4$ investigated by ^{59}Co and ^{63}Cu magnetic resonance. *J Phys-Condens Mat*. 2001;14(2):219–230.
11. Sugita H, Wada S, Yamada Y, Miyatani K, Tanaka T. NMR Investigation of an Itinerant Weakly Antiferromagnetism in Metallic Thiospinels $CoCo_2S_4$ and $(Co_{1-x}Cu_x)Co_2S_4$. *J Phys Soc Jpn*. 1998;67(4).
12. Miyatani K, Tanaka T, Sakita S, Ishikawa M, Snirakawa N. Magnetism and Superconductivity in Copper Spinels. *Jpn J Appl Phys*. 1993;32:448.
13. Fang L, Zou PY, Lu XF, *et al.* Superconductivity in thiospinel $Cu_{1.3}K_{0.2}Co_{1.5}S_4$. *Phys Rev B*. 2005;71(6):064505.
14. Toby BH, Von Dreele RB. *GSAS-II* : the genesis of a modern open-source all purpose crystallography

software package. *J Appl Crystallogr*. 2013;46(2):544–549.

15. Riedel E, Horvath E. Kationen-anionen-abstände in kupfer- und chrom-thiospinellen. *Mater Res Bull*. 1973;8(8):973–982.
16. Wohlfarth EP. Handbook of Magnetic Materials. North-Holland Publishing Company; 1982
17. Anderson PW. Generalizations of the Weiss Molecular Field Theory of Antiferromagnetism. *Phys Rev*. 1950;79(4):705–710.

FIGURE 1. (a) The crystal structure of $CuCo_2S_4$ composed of tetrahedral (CuS_4) and octahedral (CoS_6); (b) Five kinds of superexchange interactions in thiosipnel structure AB_2S_4: AB(NN), BB(NN), AB(NNN), BB(NNN) and AA(NN), only the AA(NN), i.e., Cu-S-Cu interaction, is exist in $CuCo_2S_{4-x}Se_{1-x}$ system.

FIGURE 2 (a) Powder XRD patterns of $CuCo_2S_{4-x}Se_x$ compounds, the patters indicate no impurities in these samples; (b) One, x = 0.2, of the XRD pattern Rietveld refinements; (c-d) The distance of Cu-Cu and lattice constant a as a function of different Se doping contents x, and they both increase with selenium doping increase.

FIGURE 3. SEM images with different magnification of the $CuCo_2S_4$ compounds (a) × 1.00 k, (b) × 10.00 k and SEM images of different selenium doping with magnification × 1.00 k, (c) x = 0.2, (d) x = 0.4, (e) x = 0.6, (f) x = 0.8

FIGURE 4. (a) Temperature ranged from 2 to 60 K dependence of the susceptibility χ in ZFC and FC modes at the external-field H = 200 Oe for the spinel-type $CuCo_2S_{4-x}Se_x$ (x = 0, 0.2, 0.4, 0.6, 0.8) system, and the inset shows the ZFC curves ranged from 2 to 10 K. T_{N1} is labeled for the first antiferromagnetic transition in higher temperature. T_{N2} is labeled for the new appeared antiferromagnetic transition in lower temperature in x = 0.4, 0.6, 0.8 samples. (b) Temperature ranged from 2 to 60 K dependence of 1/χ in ZFC and the fitting results of Curie-Weiss law marked with white solid line. (c) Temperature-dependent DC susceptibility χ at the external-field H = 20 Oe for the x = 0.4 and x = 0.6 samples. (d), (e) The M-H loops for x = 0.4 and x = 0.6 are obtained at 2 K, 4 K, 6 K and 10 K. The coordinate value of M is fit to the M-H curve at 2K. The other M-H curves for 4 K, 6K, and 10 K are shifted up by adding 0.1, 0.2, and 0.3 to their M values, respectively, to separate them from their heavy overlaps.

FIGURE 5. The temperature dependence of the real part (χac') in 6 Oe AC field for various values of frequency for (a) x = 0.4 and (b) x = 0.6 samples.

FIGURE 6. (a) The relationship between Néel temperature and selenium doping; (b) The relationship between Curie constant, Curie temperature and selenium doping; (c) The distance of Cu-S(Se) as a function of different Se doping contents x.

TABLE 1. The corresponding factors of all the Rietveld refinement results.

	$x = 0$	$x = 0.2$	$x = 0.4$	$x = 0.6$	$x = 0.8$
R_{wp}	1.13%	1.12%	1.18%	1.29%	1.44%
R_F	9.19%	8.72%	7.9%	7.4%	6.18%
GOF	1.18	1.19	1.19	1.36	1.48

TABLE 2. The effective Bohr magneton μ_{eff} of all samples.

	$x = 0$	$x = 0.2$	$x = 0.4$	$x = 0.6$	$x = 0.8$
C (emu·K/g·Oe)	6.6	7.4	11.1	7.6	8.5
μ_{eff} (μ_B)	0.90	0.96	1.17	0.97	1.02

TABLE 3. The data of lattice parameters, paramagnetic Curie temperatures and Néel temperatures.

x	lattice parameter (Å)	T_P (K)	T_{N1} (K)	T_{N2} (K)
0.0	9.4635	167.6	3.9	-
0.2	9.4868	162.3	5.7	-
0.4	9.5178	458.2	6.4	2.7
0.6	9.5435	213.0	6.1	3.3
0.8	9.5712	283.2	6.1	3.5

TABLE 4. Coefficient α and the angle of Cu-S(Se)-Cu for samples with doping contents x.

X	0	0.2	0.4	0.6	0.8
α	0.9550	0.9319	0.9725	0.9441	0.9579
Angle (Cu-S(Se)-Cu) / degree	77.701	77.553	77.692	77.648	77.715

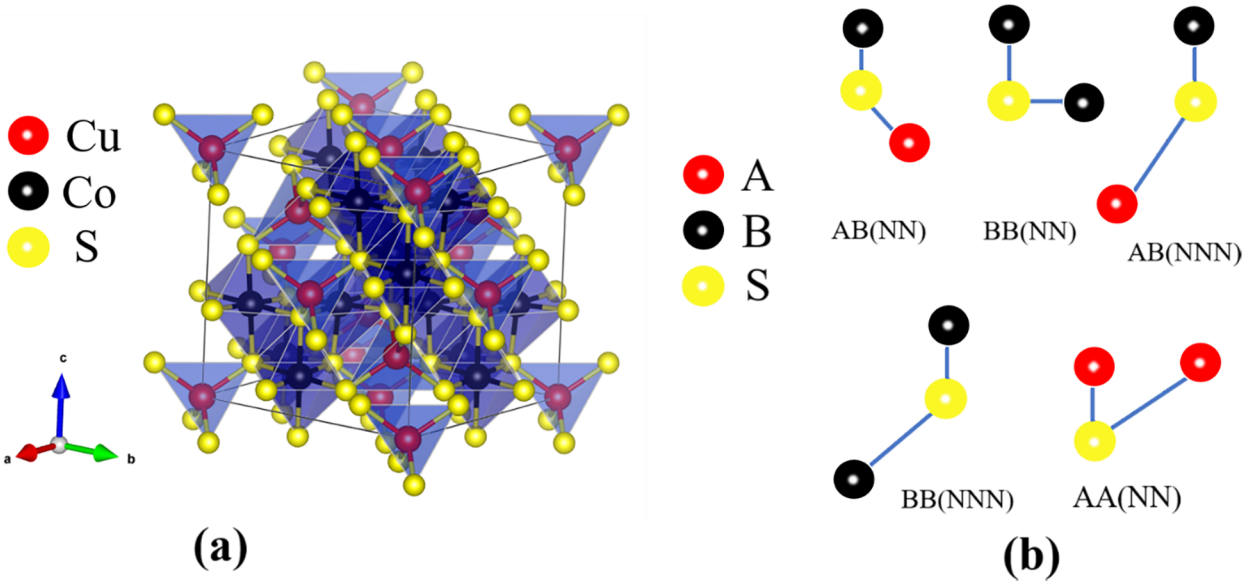

jace_17607_f1.tif

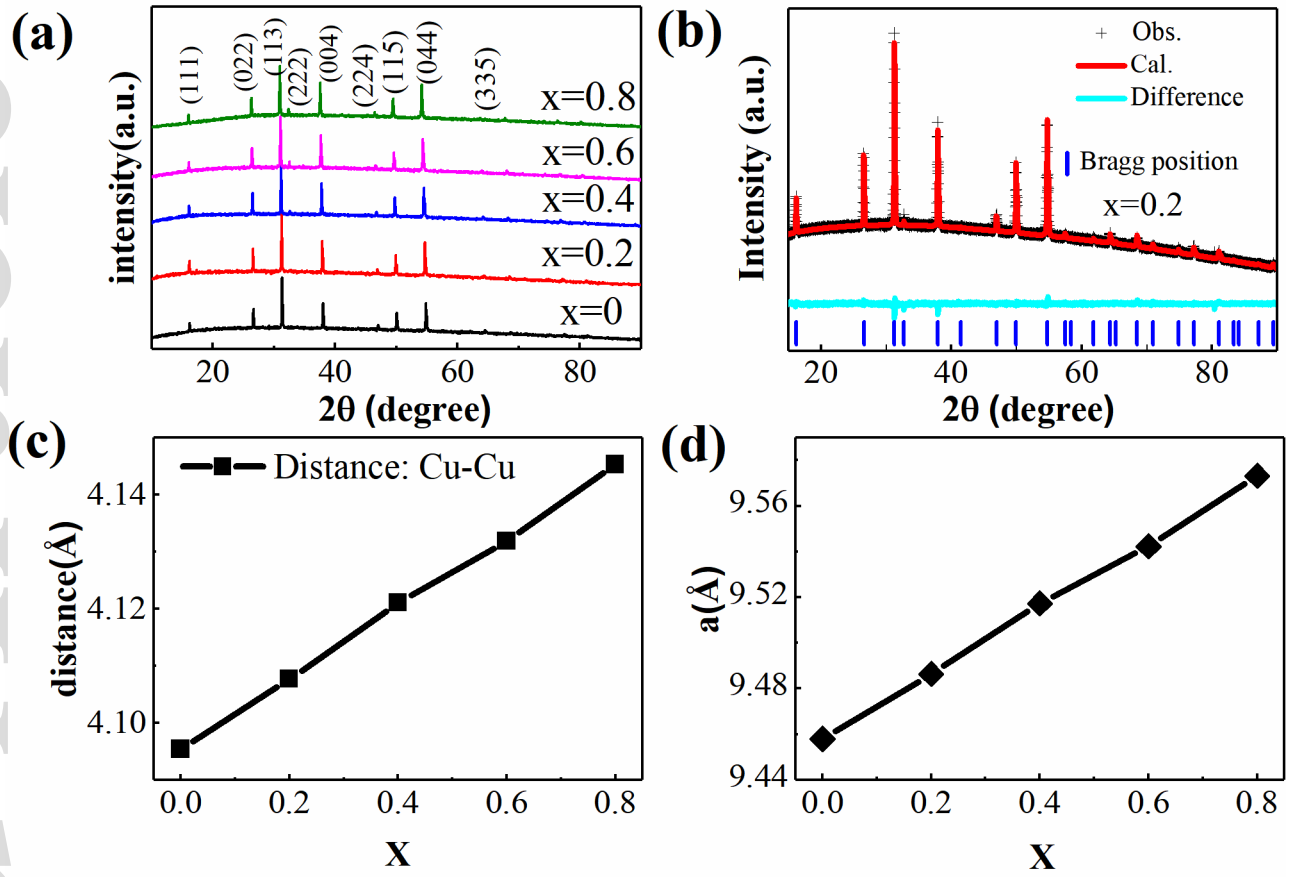

jace_17607_f2.tif

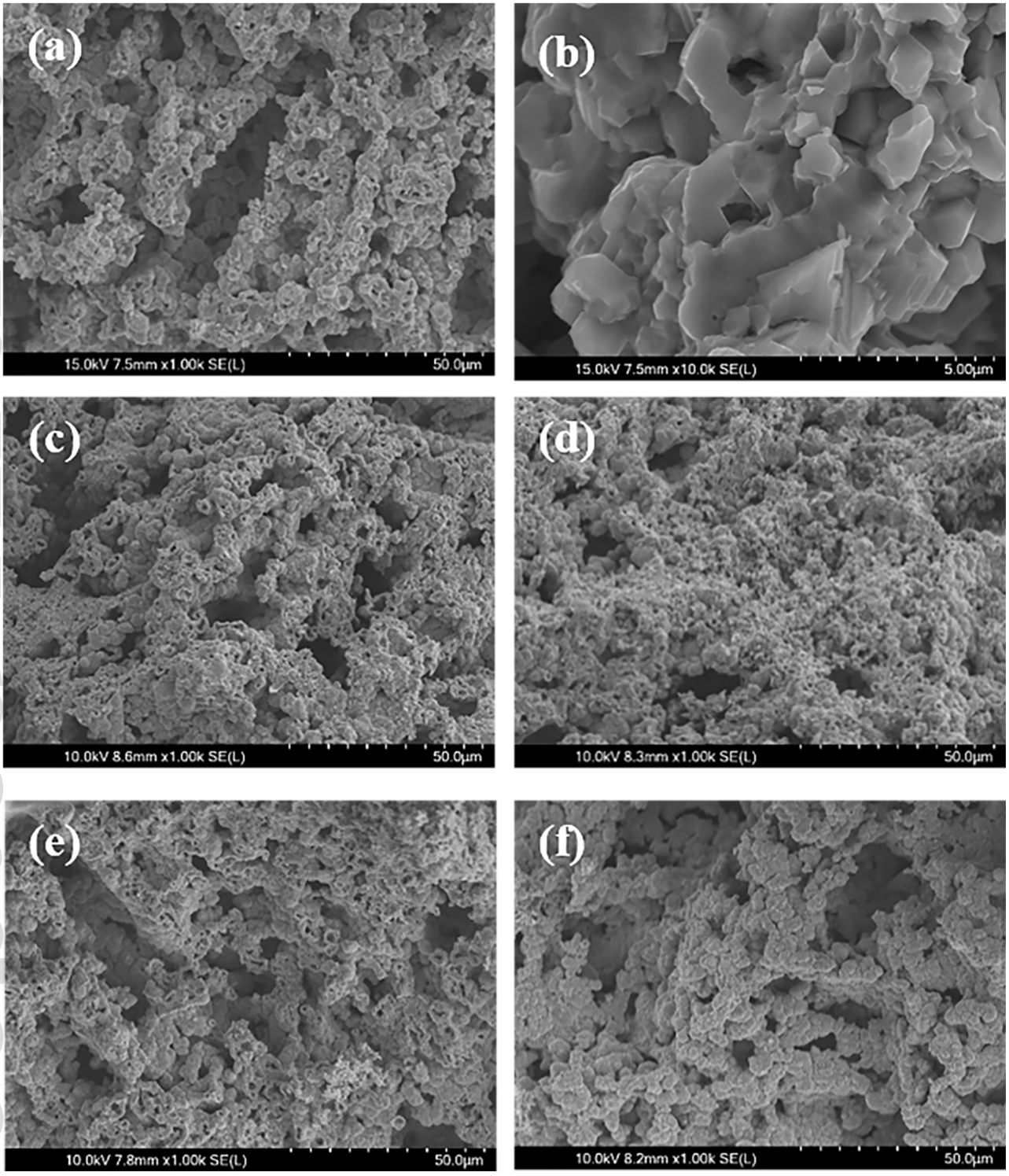

jace_17607_f3.tif

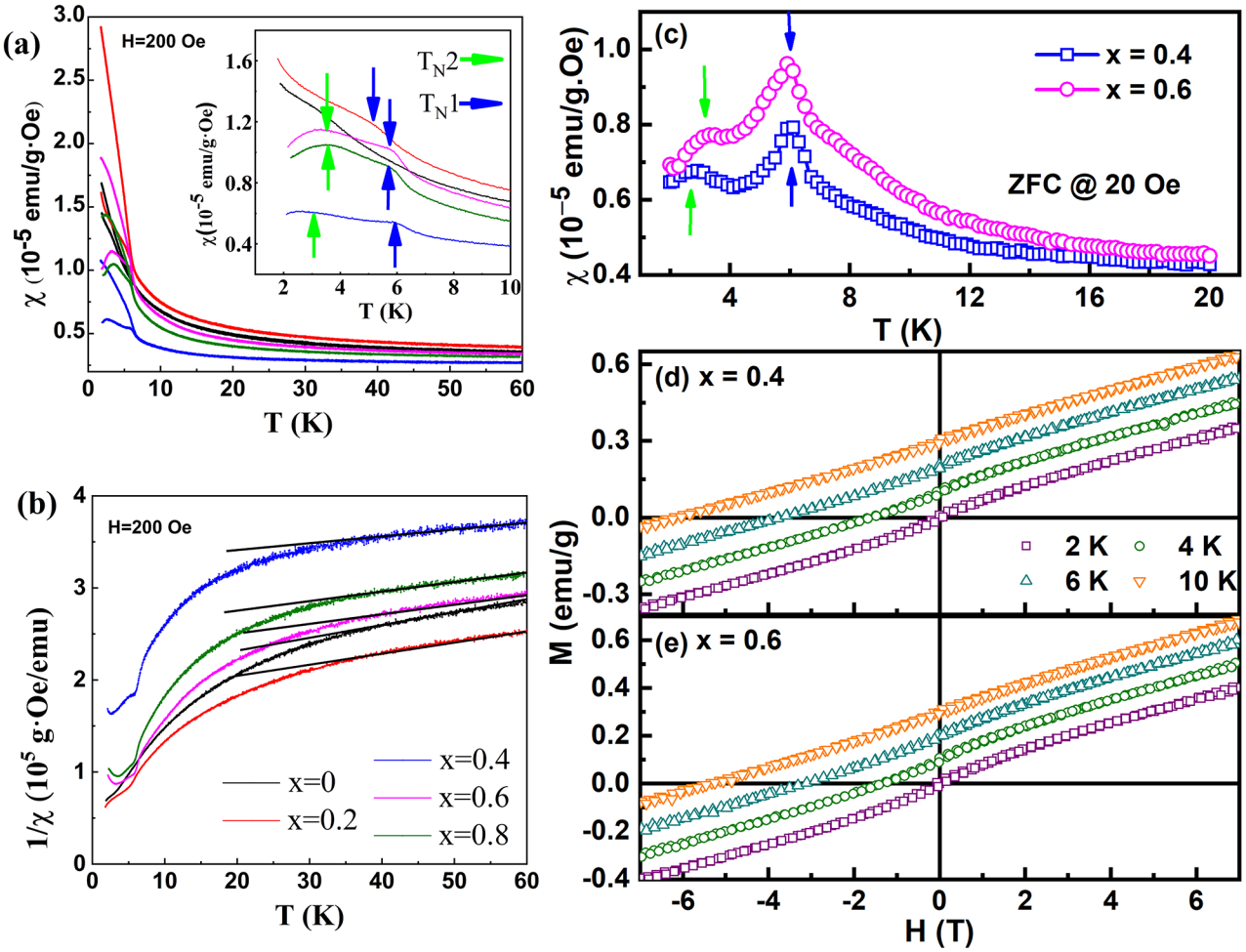

jace_17607_f4.tif

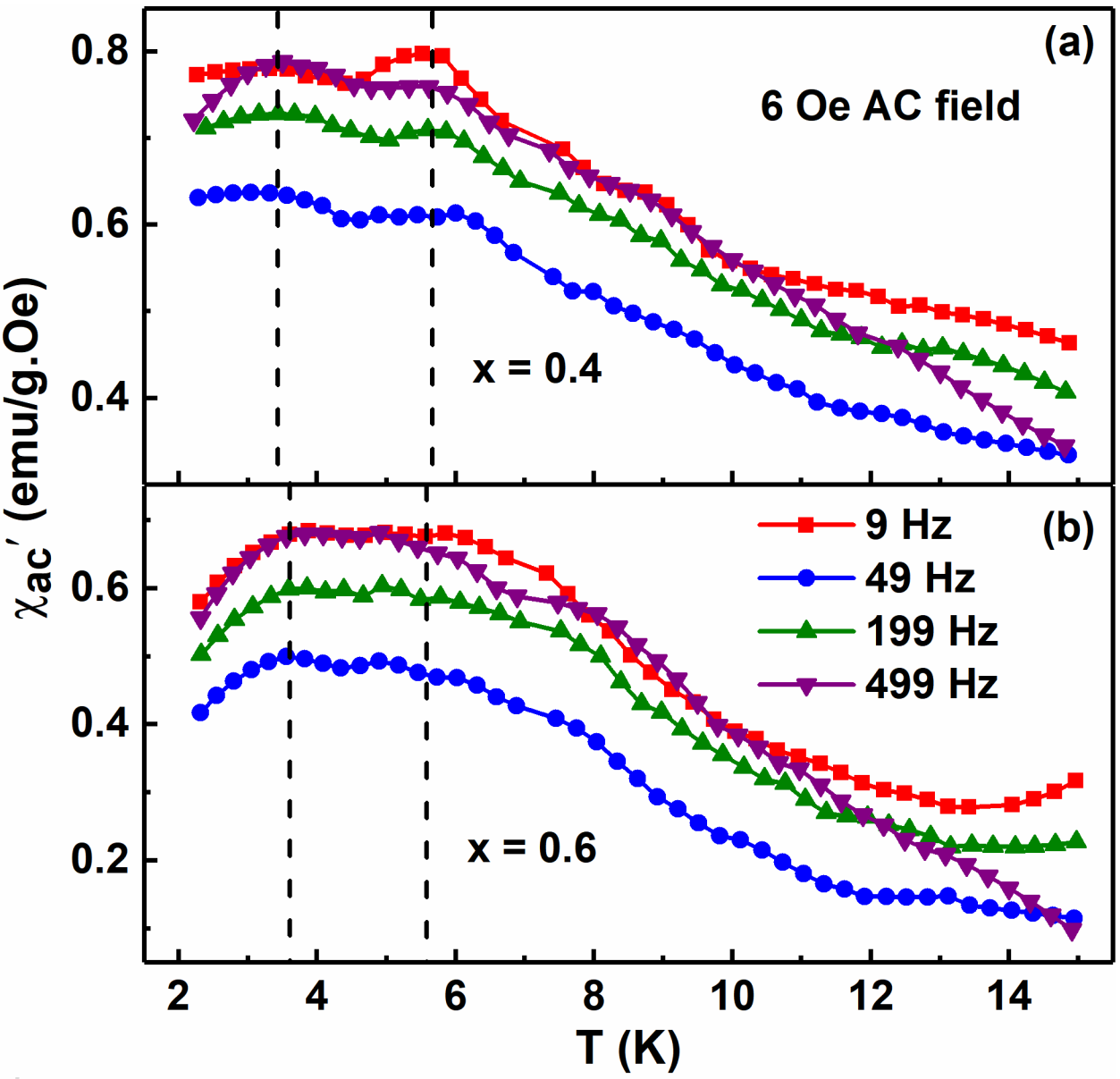

jace_17607_f5.tif